SUPPORTING INFORMATION

Ultrafast Electronic Relaxation Dynamics of Atomically Thin MoS_2 is Accelerated by Wrinkling

Ce Xu,[1] *Guoqing Zhou,*[2] *Evgeny M. Alexeev,*[3] *Alisson R. Cadore,*[3] *Ioannis Paradisanos,*[3] *Anna K. Ott,*[3] *Giancarlo Soavi,*[3] *Sefaattin Tongay,*[4] *Giulio Cerullo,*[5,6] *Andrea C. Ferrari,*[3,*] *Oleg V. Prezhdo,*[2,7,*] *and Zhi-Heng Loh*[1,*]

[1] School of Chemistry, Chemical Engineering and Biotechnology, and School of Physical and Mathematical Sciences, Nanyang Technological University, Singapore 637371, Singapore

[2] Department of Physics and Astronomy, University of Southern California, Los Angeles, California 90089, United States

[3] Cambridge Graphene Centre, University of Cambridge, Cambridge CB3 0FA, United Kingdom

[4] School for Engineering of Matter, Transport and Energy, Arizona State University, Tempe, Arizona 85287, United States

[5] Department of Physics, Politecnico di Milano, Piazza Leonardo da Vinci 32, I-20133 Milano, Italy

[6] IFN-CNR, Piazza Leonardo da Vinci 32, I-20133, Milano, Italy

[7] Department of Chemistry, University of Southern California, Los Angeles, California 90089, United States

[*] E-mail: acf26@cam.ac.uk (A.C.F.), prezhdo@usc.edu (O.V.P.), zhiheng@ntu.edu.sg (Z.-H.L.)

1. Height and width profiles of multilayer MoS_2 wrinkles

Fig. S1a is an AFM image of wrinkles in 17L-MoS_2. We select 3 wrinkles and take height profiles along 3 lines for each wrinkle (Fig. S1b).

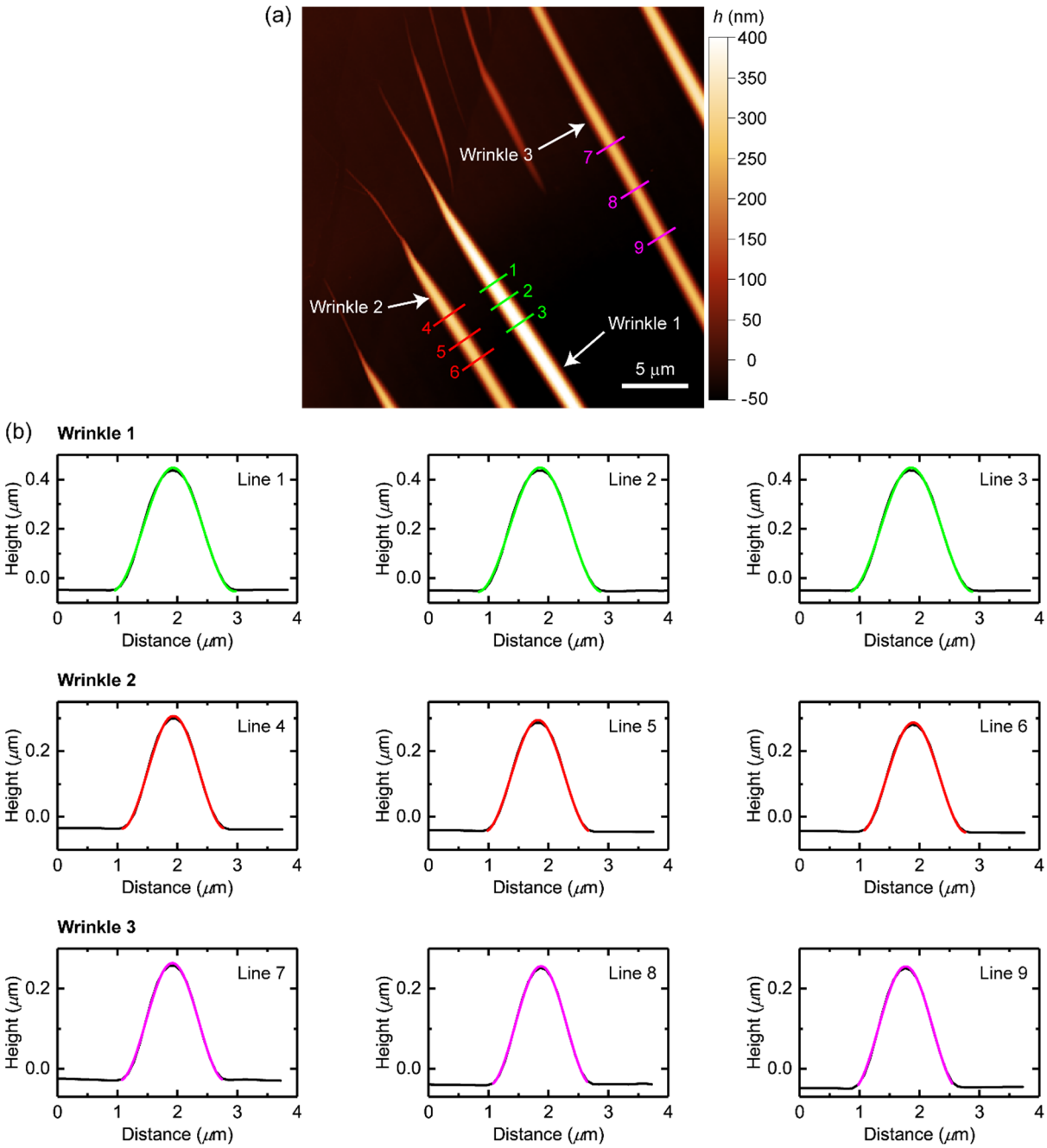

Figure S1. (a) AFM image of wrinkled 17L-MoS_2. (b) Height profiles along line 1, 2, 3 (on wrinkle 1); 4, 5, 6 (on wrinkle 2); and 7, 8, 9 (on wrinkle 3). Colored lines are fits to Eq. S1.

All height profiles are fit to the function[1]:

$$h(x) = \frac{\delta}{2}\left(1 + \cos\frac{2\pi x}{\lambda}\right) + h_0, \quad \text{(S1)}$$

where δ and λ are the height and width of the wrinkle, respectively, and h_0 is the offset. The fitting results are summarized in Table S1.

Table S1. Heights δ and widths λ of lines 1 – 9 of wrinkles 1 – 3. The errors correspond to the standard deviation.

		Line 1	Line 2	Line 3	Mean
Wrinkle 1	Height δ (μm)	0.50	0.50	0.50	0.50 ± 0.01
	Width λ (μm)	2.05	2.08	2.08	2.07 ± 0.02
		Line 4	Line 5	Line 6	Mean
Wrinkle 2	Height δ (μm)	0.34	0.34	0.33	0.34 ± 0.01
	Width λ (μm)	1.75	1.80	1.79	1.78 ± 0.03
		Line 7	Line 8	Line 9	Mean
Wrinkle 3	Height δ (μm)	0.29	0.30	0.31	0.30 ± 0.01
	Width λ (μm)	1.78	1.74	1.82	1.78 ± 0.04

2. Static PEEM image

The static PEEM image obtained with 3.61-eV illumination is shown in Fig. S2a. The image contrast between flat (bright) and wrinkled (dark) portions of 17L-MoS_2 is opposite to that expected based on topography.[2] This could be attributed to the calculated VB DOS being lower for wrinkled than for flat MoS_2 (see Fig, S2b). Thus, the photoionization cross-section is smaller for wrinkled MoS_2.

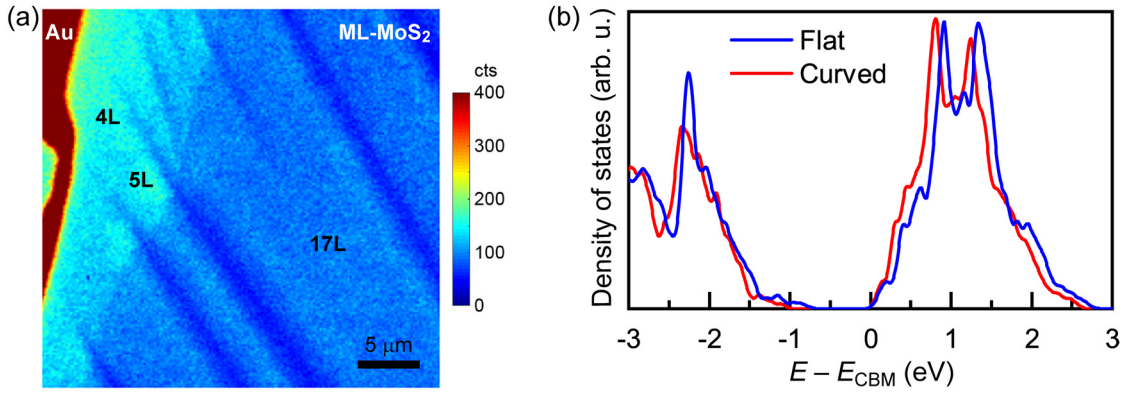

Figure S2. (a) Static PEEM image of multilayer MoS_2, comprising 4L, 5L, and 17L regions, obtained under 3.61-eV illumination. (b) Calculated density of states (DOS), showing a lower valence band DOS for curved MoS_2.

3. Determination of photon order and probe window

We perform fluence dependence measurements to determine the photon order of the 2.41-eV pump and 3.61-eV probe pulse interactions with wrinkled 17L-MoS_2. The photoemission intensity is given as[3,4]:

$$S = \sigma_{pu} \cdot F_{pu}^{N_{pu}} \times \sigma_{pr} \cdot F_{pr}^{N_{pr}}, \tag{S1}$$

where S is total photoemission signal, σ_{pu} (σ_{pr}) is the pump absorption (probe ionization) cross-section, F_{pu} (F_{pr}) is the fluence of the pump (probe) pulse, and N_{pu} (N_{pr}) is the pump (probe) photon order. Figs. S3a,b show that the PEEM signal scales linearly with pump and probe fluence, respectively. Hence, both pump and probe pulses each interact with the 17L-

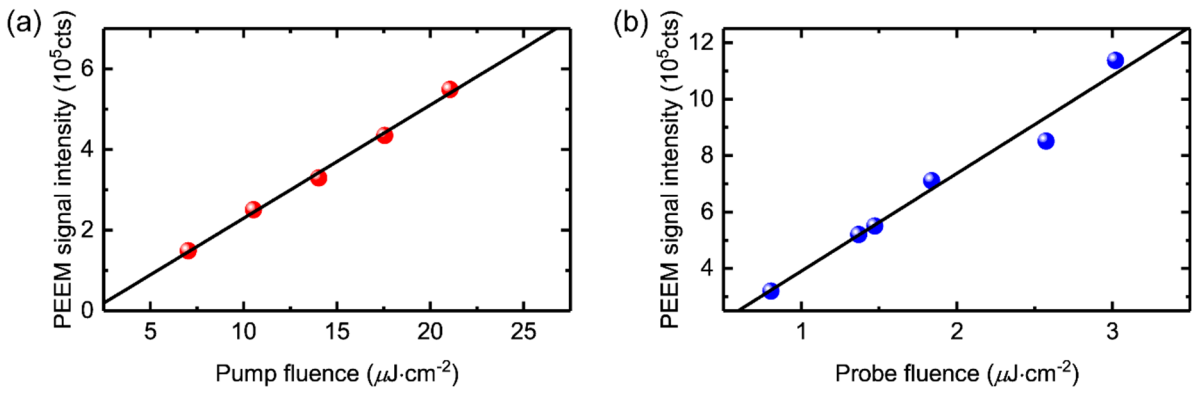

Figure S3. PEEM signal intensity as a function of (a) pump and (b) probe fluence.

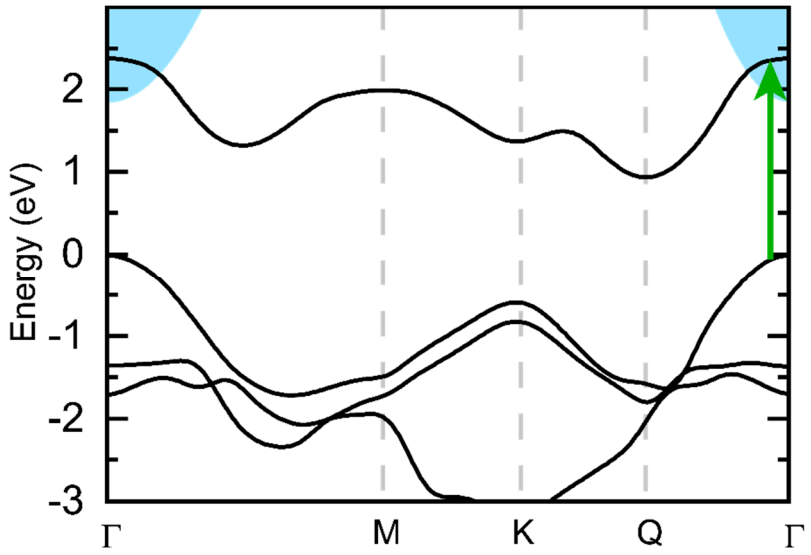

Figure S4. Band structure (from Ref. 6) of bulk MoS_2, with one-photon 2.41-eV pump (green arrow) and one-photon 3.61-eV probe window (shaded regions).

MoS_2 sample *via* a one-photon process.

The probe photon order is used to establish the probe window (Fig.S4). In photoemission, the probe window arises from the requirement to conserve in-plane momentum[5], and defines the region of the band structure from which e can be ejected.[5] The band structure from Ref. 6 is for b-MoS_2 in vacuum, calculated within the G_0W_0 approximation.

To enable comparison with our experiments, we shift the lowest-energy CB to reproduce the experimental K_v–K_c band gap of 1.95eV.[7] We also use the experimental ionization energy~5.47eV[8] for b-MoS_2 to determine the photoemission probe window.

4. Extended time traces of the wrinkled and flat regions of multilayer MoS_2

Fig. 4c shows the time traces of wrinkled and flat regions of the 17L-MoS_2 sample over a time delay range of 0 – 0.5 ps so that their different decay dynamics can be clearly seen. Here, we show the time traces over an extended range of –0.5 – 1.5ps. Those of wrinkled (Fig. S5a) and flat 17L-MoS_2 (Fig. S5b) are fit to one single exponential decay at positive time delay and

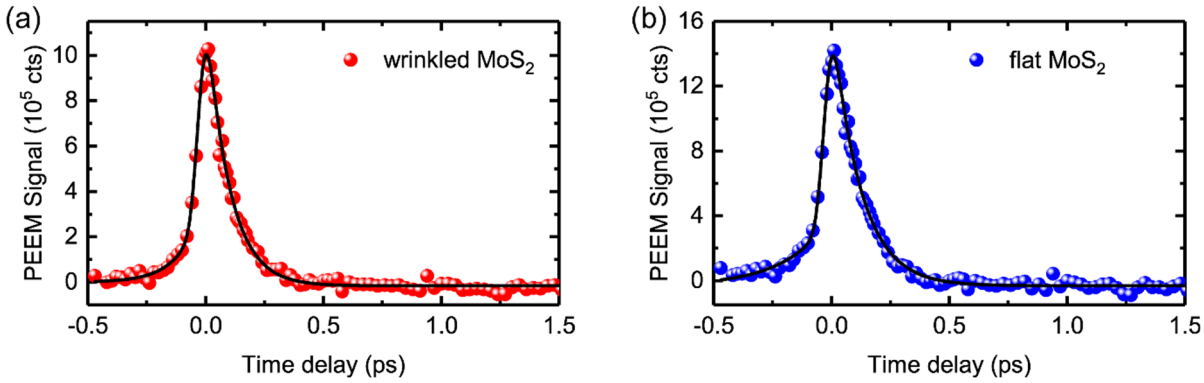

Figure S5. Extended TR-PEEM time traces of (a) wrinkled and (b) flat 17L-MoS_2.

another at negative time delay, both convolved with the instrumental response function. At negative time delay, the 3.61-eV pulse serves as the photoexcitation pump pulse, whereas the 2.41-eV pulse serves as the photoionization probe pulse, reversing the roles of these two pulses at positive time delays. The decay observed at negative time delays therefore arises from dynamics induced by 3.61-eV excitation.

5. Distributions of time constants for other wrinkles

The histogram of lifetimes for wrinkle 1 is in Fig. 5b. From the lifetime map (Fig.S6a), we

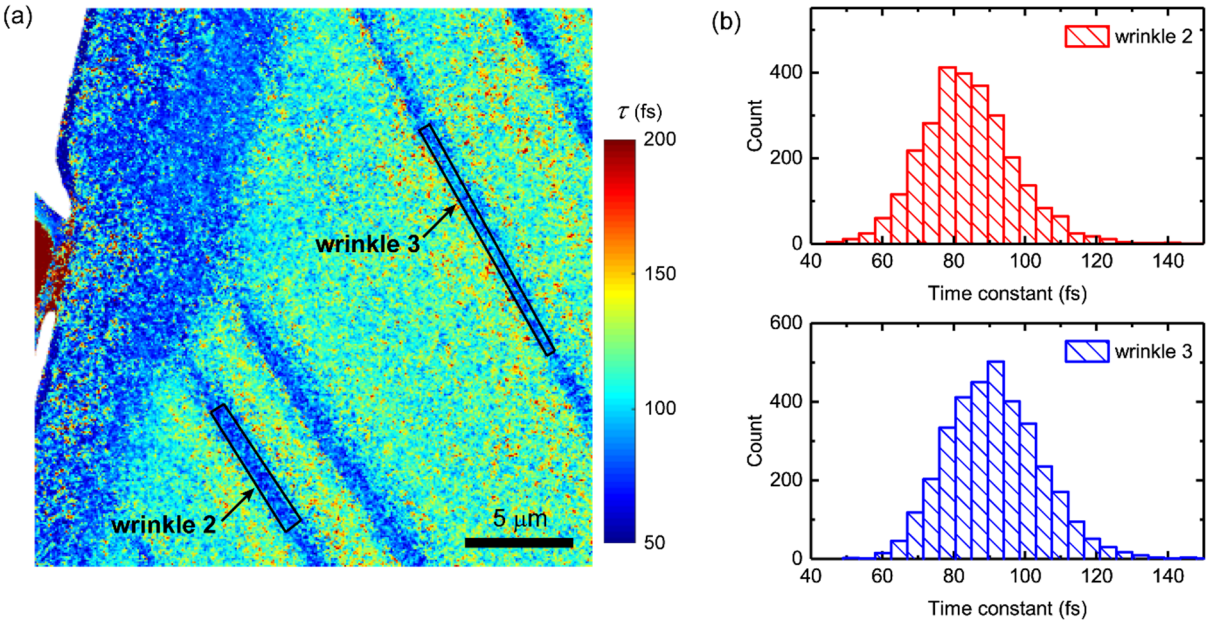

Figure S6. (a) Lifetime map of the electronic relaxation dynamics of 17L-MoS_2. (b) Histograms of time constants for wrinkles 2 (top panel) and 3 (bottom panel).

extract the distributions of time constants for the other two wrinkles (Fig.S6b). For wrinkles 2 and 3, these are characterized by mean values (standard deviations) of 84 fs (13 fs) and 91 fs (14 fs), respectively. Both wrinkles undergo faster electronic relaxation than the flat region, consistent with the result obtained for wrinkle 1.

6. Electronic structure of a larger wrinkled MoS_2 model

Two additional periodic systems, 50% larger than the models in the main text (Figs. 6a,b), are examined to validate the impact of wrinkles on electronic structure. Flat and curved B-MoS_2 are represented with rectangular simulations cells comprising 1×15×1 unit cells (Figs. S7a,b). The flat B-MoS_2 (System C) extends along the armchair direction with 81.7-Å length (Fig. S7a). The same method to create the wrinkled system in the main text is used to build one with a wave shape (System D, Fig. S7b). This has a 50 Å radius of curvature along the armchair direction, and its length is reduced to 79.4 Å with the thickness increased to 6.54 Å for each monolayer. The curvature of the B-MoS_2 model system D is twice smaller than Fig. 6b.

The geometry optimization is performed with VASP,[9-11] in the same way as described in the main text, employing the PBE exchange−correlation functional,[12] the PAW method,[13]

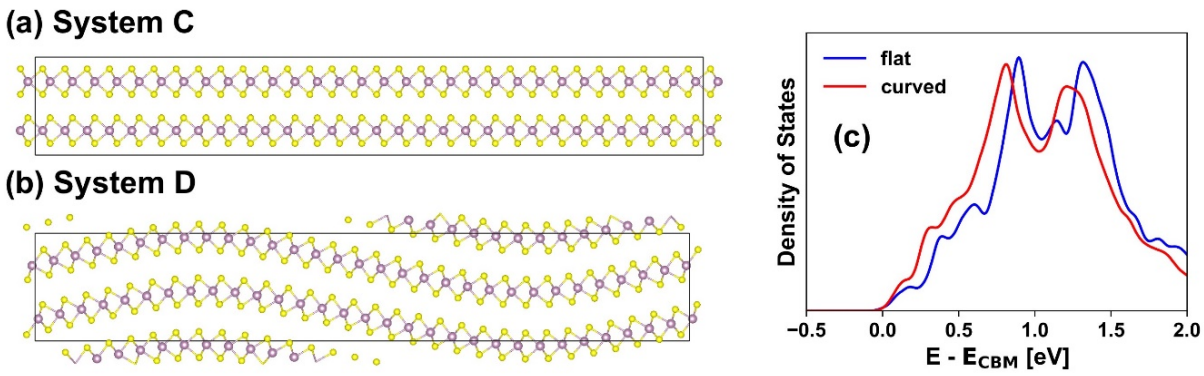

Figure S7. Side views of optimized (a) flat and (b) curved B-MoS_2. System D is curved along the armchair direction of B-MoS_2. The box shows the supercell boundary in the calculation. (c) Electronic DOS for C and D, aligned to the CB edge.

and the DFT-D3 van der Waals correction.[14,15] The Brillouin zone is sampled with 7×1×3 Γ-centered Monkhorst-Pack grids, the energy cutoff for the plane wave basis is set to 340 eV, and the convergence criterion of geometry optimization on atomic forces is 0.001 eV/Å. After geometry optimization, the radius of curvature for the wrinkled b-MoS_2 increases to 58 Å. Using the optimized structures, we compute the electronic DOS. The Brillouin zone sampling is increased to use 17×1×5 Γ-centered Monkhorst-Pack grids. Fig. S6c indicates that the DOS of the curved system D rises faster from the CB edge, similar to the DOS observed for the smaller models in the main text (Fig. 6c). Because the NA coupling is inversely proportional to the energy gap, Eq. 2, it is larger in regions of higher DOS. The nonradiative e-ph relaxation is faster when DOS is higher.[16,17] Therefore, the conclusions from the NAMD simulation with the smaller b-MoS_2 model hold for the larger one as well.

References

(1) Vella, D.; Bico, J.; Boudaoud, A.; Roman, B.; Reis, P. M. The Macroscopic Delamination of Thin Films from Elastic Substrates. *Proc. Natl. Acad. Sci. U.S.A.* **2009**, *106* (27), 10901-10906.

(2) Rempfer, G. F.; Nadakavukaren, K. K.; Griffith, O. H. Topographical Effects in Emission Microscopy. *Ultramicroscopy* **1980**, *5* (4), 437-448.

(3) Wang, L.; Xu, C.; Li, M. Y.; Li, L. J.; Loh, Z.-H. Unraveling Spatially Heterogeneous Ultrafast Carrier Dynamics of Single-Layer WSe_2 by Femtosecond Time-Resolved Photoemission Electron Microscopy. *Nano Lett.* **2018**, *18* (8), 5172-5178.

(4) Xu, C.; Yong, H. W.; He, J.; Long, R.; Cadore, A. R.; Paradisanos, I.; Ott, A. K.; Soavi, G.; Tongay, S.; Cerullo, G.; Ferrari, A. C.; Prezhdo, O. V.; Loh, Z.-H. Weak Distance Dependence of Hot-Electron-Transfer Rates at the Interface between Monolayer MoS_2 and Gold. *ACS Nano* **2021**, *15* (1), 819-828.

(5) Hüfner, S. *Photoelectron Spectroscopy: Principles and Applications*; Springer, 2013.

(6) Molina-Sánchez, A.; Sangalli, D.; Hummer, K.; Marini, A.; Wirtz, L. Effect of Spin-Orbit Interaction on the Optical Spectra of Single-Layer, Double-Layer, and Bulk MoS_2. *Phys. Rev. B* **2013**, *88* (4), 045412.

(7) Grubišić Čabo, A.; Miwa, J. A.; Grønborg, S. S.; Riley, J. M.; Johannsen, J. C.; Cacho, C.;

Alexander, O.; Chapman, R. T.; Springate, E.; Grioni, M.; Lauritsen, J. V.; King, P. D. C.; Hofmann, P.; Ulstrup, S. Observation of Ultrafast Free Carrier Dynamics in Single Layer MoS_2. *Nano Lett.* **2015**, *15* (9), 5883-5887.

(8) Schlaf, R.; Lang, O.; Pettenkofer, C.; Jaegermann, W. Band Lineup of Layered Semiconductor Heterointerfaces Prepared by Van Der Waals Epitaxy: Charge Transfer Correction Term for the Electron Affinity Rule. *J. Appl. Phys.* **1999**, *85* (5), 2732-2753.

(9) Kresse, G.; Hafner, J. Ab Initio Molecular-Dynamics Simulation of the Liquid-Metal–Amorphous-Semiconductor Transition in Germanium. *Phys. Rev. B* **1994**, *49* (20), 14251.

(10) Kresse, G.; Furthmuller, J. Efficient Iterative Schemes for Ab Initio Total-Energy Calculations Using a Plane-Wave Basis Set. *Phys. Rev. B* **1996**, *54* (16), 11169-11186.

(11) Kresse, G.; Furthmuller, J. Efficiency of Ab-Initio Total Energy Calculations for Metals and Semiconductors Using a Plane-Wave Basis Set. *Comput. Mater. Sci.* **1996**, *6* (1), 15-50.

(12) Perdew, J. P.; Burke, K.; Ernzerhof, M. Generalized Gradient Approximation Made Simple. *Phys. Rev. Lett.* **1996**, *77* (18), 3865-3868.

(13) Blochl, P. E. Projector Augmented-Wave Method. *Phys. Rev. B* **1994**, *50* (24), 17953-17979.

(14) Grimme, S.; Antony, J.; Ehrlich, S.; Krieg, H. A Consistent and Accurate Ab Initio Parametrization of Density Functional Dispersion Correction (DFT-D) for the 94 Elements H-Pu. *J. Chem. Phys.* **2010**, *132* (15), 154104.

(15) Grimme, S.; Ehrlich, S.; Goerigk, L. Effect of the Damping Function in Dispersion Corrected Density Functional Theory. *J. Comput. Chem.* **2011**, *32* (7), 1456-1465.

(16) Akimov, A. V.; Prezhdo, O. V. The PYXAID Program for Non-Adiabatic Molecular Dynamics in Condensed Matter Systems. *J. Chem. Theory Comput.* **2013**, *9* (11), 4959-4972.

(17) Akimov, A. V.; Prezhdo, O. V. Advanced Capabilities of the PYXAID Program: Integration Schemes, Decoherence Effects, Multiexcitonic States, and Field-Matter Interaction. *J. Chem. Theory Comput.* **2014**, *10* (2), 789-804.